Magnetic Properties of Quasi-Two-Dimensional Non-Kramers Magnets TmX_3 and TmOX (X = Cl, Br, I)

Shreenithi Sai Katta
School of Physics, Georgia Institute of Technology, Atlanta, GA 30332, USA
(Dated: December 10, 2024)

I. INTRODUCTION

Condensed matter physics seeks to understand the behavior of quantum matter and how such behavior emerges from interactions between assemblies of atoms for technological applications. Magnetism is a central phenomenon in this field, and the search for exotic magnetic behavior in materials is a very active area of inquiry. A key question is how microscopic quantum mechanical effects — spin interactions — between magnetic dipole moments — spins — yield the magnetic properties and structure of specific materials and compounds.

The elusive quantum spin liquid phase is a fascinating example of the many complex magnetic phases that are, in principle, possible. This phase is stabilized by competing interactions that prevent magnetic ordering down to exceptionally low temperatures. Instead of breaking symmetries associated with the crystal lattice and the choice of spin orientations, quantum spin-liquids are quantum superpositions of many classically degenerate spin configurations. The resulting entanglement leads to possible applications in quantum information and computing where entanglement is essential to protect information as it travels through a channel. Although experimental work has not yet realized a quantum spin liquid for applications, the chase toward candidate materials has led to an explosion in the structural and magnetic characterization of many compounds with tunable magnetic interactions. Two-dimensional lattices are a particularly interesting class of magnets for their dominating spin interactions within a two-dimensional plane and weak interactions between planes. Specifically, van der Waals materials comprised of lanthanide atoms offer the possibility of obtaining clean 2D magnets with controllable magnetic anisotropies and interactions. These conditions are necessary for stabilizing a quantum spin liquid and could open the door to a whole new family of quantum spin liquid candidates. However, even some of the simplest members of this material family, such as LnX_3 and LnOX (X = Cl, Br, I), remain poorly characterized.

The trivalent lanthanides, or rare-earths ions Ln^{3+}, have large atomic magnetic moments originating from the interactions between electrons in partially filled $4f$ orbitals. These multi-electron configurations often yield singlet (non-Kramers), doublet (Kramers), or quartet ground-states under the influence of spin-orbit coupling and degeneracy-lifting crystal field effects. Coupled with halides (Cl, Br, I) and chalcogenide (O) ligands, trivalent rare-earth ions crystallize into quasi-2D structures to form LnX_3 and LnOX families (X = Cl, Br, I). Thirteen trivalent lanthanide elements have magnetic moments. Of these thirteen, twelve have stable isotopes that can be utilized under laboratory conditions. Eleven of these stable isotopes have some reports on their crystal structure, magnetic susceptibility, and neutron diffraction properties for either LnX_3 or LnOX as seen in Table I [1–4]. The remaining stable isotope species, thulium (Tm^{3+}), has little to no information on its crystal structure, magnetic susceptibility and neutron diffraction patterns for either TmX_3 and TmOX. Unlike more investigated Yb^{3+} and Dy^{3+} systems, Tm^{3+} are non-Kramers ions, offering the possibility for singlet or quasi-doublet single-ion ground states prone to quantum fluctuations.

Therefore, this project seeks to fill the knowledge gap by completing characterization work on the TmX_3 and TmOX compounds. Characterization entails x-ray diffraction measurements to identify the crystal lattice structure and its symmetries, magnetic susceptibility to identify the magnetic interactions, low-temperature heat capacity to observe putative magnetic ordering and phase transitions, and neutron diffraction and scattering to establish magnetic structure and crystal field excitations. Here, we report the complete characterization of $TmBr_3$ and TmI_3 using the aforementioned methods. Both materials crystallize into the $R\bar{3}$ space group with antiferromagnetic signatures present in magnetization measurements. Neutron diffraction reveals a magnetic ordering transition in both compounds around 1 Kelvin that is corroborated by heat capacity measurements. The entropy release across the transition in TmI_3 is anomalously low, pointing towards crystal field or impurity effects. Partial characterization was completed on TmOBr using x-ray diffraction, magnetic susceptibility, and heat capacity, showing both an antiferromagnetic signature and a phase transition around 1 Kelvin similar to $TmBr_3$ and TmI_3.

II. BACKGROUND

The rare earth elements provide a foundation for exotic magnetic behavior given their large, anisotropic magnetic moments and potentially novel ground states. Specifically, the rare-earth trihalide and oxyhalide families have been of heavy importance in the search for Kitaev spin systems and quantum spin liquids. Their two dimensionality leads to weak next nearest neighbor interactions between planes, creating anisotropic exchange interactions that can be studied further. Lanthanide chlorides and select oxychlorides have been studied at length

TABLE I: List of LnX_3 and LnOX compounds as reported on in literature with their reported crystal structure (space group), magnetic ordering (antiferromagnetic or ferromagnetic), ordering temperature, Weiss temperature, and whether neutron diffraction has been done.

Compound	Space Group	Reference	Magnetic Ordering	Ordering Temp (K)	θ_{CW}	Neutron
$CeCl_3$	$Cmcm$	[5–8]	AFM	0.11	-0.125 ± 0.01	-
$CeBr_3$	$C6_3/m$	[1, 9]	AFM Ising/FM XY	-	-0.050 ± 0.045	-
CeI_3	-	-	-	-	-	-
$PrCl_3$	$C6_3/m$	[1, 8]	AFM	0.41	0.50 ± 0.05	-
$PrBr_3$	$C6_3/m$	[1]	-	-	-	-
$NdCl_3$	$C6_3/m$	[1]	AFM	0.17-0.30 [a]	-	-
$NdBr_3$	$Ccmm$	[1, 10]	AFM	-	-	-
$SmCl_3$	-	[1, 8]	AFM	-	0.02 ± 0.01	-
$SmBr_3$	$Ccmm$	[10]	-	-	-	-
$EuCl_3$	-	-	-	-	-	-
$GdCl_3$	-	[11, 12]	FM	2.20	-	-
$GdBr_3$	$P3_112/P3_212$	[12, 13]	AFM	2.0	1 ± 1	-
GdI_3	-	[12]	-	< 1	-	-
$TbCl_3$	$Cmcm$	[14, 15]	FM	-	3.70 ± 0.05	Yes
$TbBr_3$	$R\bar{3}$	[16]	-	-	-	-
$DyCl_3$	$Cmcm$	[2, 5, 17]	-	-	-	No
$DyBr_3$	$R3$	[18–20]	-	-	-	high temp: [20]
DyI_3	$R3$	[18–20]	-	-	-	high temp: [20]
$HoCl_3$	-	-	-	-	-	-
$ErCl_3$	$C2/m$	[3]	AFM	0.350	-	Yes
$ErBr_3$	$R\bar{3}$	[3, 16]	AFM	0.280	-	Yes
ErI_3	$R\bar{3}$	[3]	AFM	0.280	-	Yes
$TmBr_3$	$R\bar{3}$	[16]	-	-	-	-
$YbCl_3$	$C2/m$	[4]	-	1.20 (SRO) 0.60 (LRO)	$-9(1)$ (c) -6.1 (ab)	Yes
$YbBr_3$	$R\bar{3}$	[16]	AFM	-	-	Yes
YbI_3	$R\bar{3}$	[21]	-	0.95 (SRO) 0.60 (LRO)	$-10 \perp ab, -7 \| ab$	Yes
CeOCl	$P4/nmm$	[22–24]	-	-	0	-
CeOBr	$P4/nmm$	[25]	-	-	-27.9	-
PrOCl	$P4/nmm$	[22, 24]	-	-	-18.80	-
PrOBr	$P4/nmm$	[25]	-	-	-24.3	-
NdOCl	$P4/nmm$	[22–24]	-	1.5	-28.7 ± 0.3	-
NdOBr	$P4/nmm$	[25]	-	-	-34.0	-
SmOCl	$P4/nmm$	[23, 24, 26]	-	8	-	-
SmOBr	$P4/nmm$	[25]	AFM	5	(-2884)[b]	-
EuOCl	$P4/nmm$	[24]	-	-	-	-
EuOBr	$P4/nmm$	[25]	-	-	(-334)[b]	-
GdOCl	$P4/nmm$	[23, 24, 26]	-	5	-10.6 ± 0.1	-
GdOBr	$P4/nmm$	[25]	-	-	-	-
TbOCl	$P4/nmm$	[22, 24]	-	-	-11.21	-
TbOBr	$P4/nmm$	[25]	-	-	-20.1	-
DyOCl	$P4/nmm$	[22–24]	AFM	11	-13.0 ± 0.3	-
DyOBr	$P4/nmm$	[25]	AFM	8	-16.2	-
HoOCl	$P4/nmm$	[22, 24]	-	-	-9.62	-
HoOBr	$P4/nmm$	[25]	-	-	-9.1	-
ErOCl	$R\bar{3}m$	[27]	-	-	-	-
ErOBr	$P4/nmm$	[25]	-	-	-13.1	-
TmOCl	$R\bar{3}m$	[27]	-	-	-	-
TmOBr	$P4/nmm$	[25]	-	-	-23.8	-
YbOCl	$R\bar{3}m$	[26]	-	-	-1.22 (c) -6.15 (ab)	-
YbOBr	$P4/nmm$	[25]	-	-	-46.3	-

Note: All information was sourced to the best abilities but this table is in no means comprehensive. Compounds and information not included were not found given limitations in searches and time

[a] Colwell and Mangum predict there is an onset of long-range order within this range based on NQR measurements as heat capacity only shows a broad anomaly [1].

[b] Fitted Curie-Weiss temperatures were determined to be unreasonable and should be interpreted with caution [3].

since the 1960s using x-ray diffraction, magnetic susceptibility, heat capacity, neutron diffraction, and computational calculations as seen in Table I. Though some materials of this family have been in the spotlight, many have been unexplored, creating a gap in the literature. This project conducted between August 2022 and December 2024 focuses on the thulium compounds TmX_3 and TmOX, a family of materials severely understudied. Given thulium is a heavy lanthanide, there is opportunity to find characteristic anisotropic magnetic moments and other novel magnetic behaviors.

A. LnX_3

The LnX_3 compounds have been studied for their crystal structure, large anisotropic magnetic moments, and possible realization of the Ising linear chain model [6]. Their simple crystal structure provides an insight into the exchange interactions of the $4f$ orbitals without overcomplicating the analysis.

1. *Crystal Structure*

The LnX_3 family crystallizes into similar structures given all lanthanides carry valence electrons in the $4f$ shell. According to Zachariasen and Morosin, lanthanide materials with less than half full valence electrons — $LaCl_3$, $CeCl_3$, $PrCl_3$, NdCl3, $LaBr_3$, $CeBr_3$, $PrBr_3$, $EuCl_3$ and $GdCl_3$ — crystallize into the UCl_3 crystal structure or the $C6_3/m$ or $P6_3/m$ hexagonal space group [28, 29]. Given their shared structure, the lattice parameters change as expected as the atomic number and valence shell increases: there is an increase in the c axis across the table and two trends in the a axis values [29]. While the c axis trend is expected, two trends in the a axis values hint at other physics such as crystal field and spin orbit coupling at play.

Heavier lanthanides from Tb to Lu are of different structures. $TbCl_3$ has been found to follow the $PuBr_3$ structure in the Cmcm space group that is commonly found in lanthanide bromides and iodides [14]. This is an outlier given other $LnCl_3$ materials follow the UCl_3 crystal structure and the YCl_3 cubic structure. For instance, $ErCl_3$ follows this trend given its $AlCl_3$ or YCl_3 like structure. However, $ErBr_3$ and ErI_3 have the BiI_3 2D hexagonal structure [3]. This once again hints at other interactions and coupling at play. Though the LnX_3 family fills its $4f$ shell, changing the lanthanide and the halide can result in subtle, but significant changes in crystal structure across the periodic table. This difference in crystal structure can yield different magnetic interactions and exchange frustration. Materials of the same family with different crystal structures provide a basis to understanding the geometric frustration introduced in magnetic interactions.

2. *$LnCl_3$ Magnetic Structure: Ising Linear Chain*

The earlier $LnCl_3$ materials show nearest neighbor antiferromagnetic ordering dominating over next nearest neighbor ferromagnetic interactions. Many conform to the 1D Ising linear chain model along the c axis characterized by decoupled, antiferromagnetic chains. These 1D chains are limited to short-range ordering because of the comparatively weak interaction between them. Evidence of this behavior can be seen in $CeCl_3$, $PrCl_3$, $NdCl_3$, and $SmCl_3$ that show short range ordering characteristic of the antiferromagnetic chains [1, 30]. Low temperature heat capacity of $NdCl_3$ explicitly demonstrates this behavior with the absence of long-range ordering however $PrCl_3$ deviates from this behavior with evidence of long-range ordering. This deviation is further emphasized during magnetic modeling of the materials. Despite the qualitative evidence of the 1D chain model, there were issues fitting data to the 1D linear chain model with multiple peaks in the data thrown out due to crystal impurities [1]. However, the same conclusions about ordering behavior are echoed with the same materials in other parts of literature.

All materials show the expected antiferromagnetic departure in the magnetic susceptibility, except $NdCl_3$ which shows ferromagnetic behavior [8]. Here, there is a discrepancy between conclusions about the interactions: Eisenstein claims the nearest neighbor interactions dominate with ferromagnetic ordering creating linear chains along the c axis, despite clear antiferromagnetic departures. Another discrepancy arises from the use of the linear Ising chain model itself. $CeCl_3$ indicated antiferromagnetic ordering at 0.11 K yet the interactions cannot be modeled by a linear chain nor an xy model. Landau attempts to use a 3D Ising chain model and Pistawala attempts to continue this exploration with high temperature data, yet neither draw conclusions [6, 7]. The uncertainty raises the question as to what leads to the different magnetic models in materials of similar crystal structures and magnetic interactions. Further deviation from the Ising linear chain model can be seen in other compounds as well.

3. *$LnCl_3$ Outliers to the Ising Linear Chain Model*

Outliers to the linear Ising chain model within the $LnCl_3$ family include $GdCl_3$, $TbCl_3$, $ErCl_3$, and $YbCl_3$. Despite having the same crystal structure as $CeCl_3$, $PrCl_3$, and $NdCl_3$, $GdCl_3$ has limited information on its potential magnetic models. Hovi reports on a second order magnetic transition at low temperature and Kotzler discusses magnetization along the c axis via dipole interaction yet neither mentions a model [12, 31]. Neutron diffraction analysis fails to provide an analytical magnetic model as well [31]. Given its unique electron configuration that mimics $CeCl_3$, $GdCl_3$ could also walk the line between a linear Ising model, xy model, and 3D Ising

model. $TbCl_3$ with its unique crystal structure similar to the bromides and iodides also deviates from the linear Ising chain model. Neutron diffraction studies show long range ferromagnetic ordering within the planes along the *a* axis which differs from the antiferromagnetic ordering along the *c* axis of its siblings [15]. This behavior can possibly be attributed to its unique crystal structure and the non-Kramers singlet ground state. Since $TbCl_3$ is known to have a crystal structure similar to the bromides and iodides, its deviations from the magnetic models that define the $LnCl_3$ family could be a key to describing the $LnBr_3$ and LnI_3 families.

Lastly, both $ErCl_3$ and $YbCl_3$ show deviations from the Ising linear chain model. Once again, it is important to remember these materials deviate from the hexagonal space group of the lighter lanthanides. $ErCl_3$ indicates short range magnetic ordering within the plane like that found in $TbCl_3$. Single crystal neutron diffraction indicates clear antiferromagnetic structures in each sublattice that is echoed in $YbCl_3$ [3]. Xing reports the characteristic strong magnetic anisotropy of $YbCl_3$ with short range ordering at 1.2 K and possible long-range ordering below 0.6 K [4]. Here, antiferromagnetic ordering occurs along the *ac* plane with stacking along the *c* axis rather than the expected *ab* plane. Though the materials are similar in crystal structure and somewhat agree in ordering within planes, there is still a discrepancy in whether that is the *ab* or *ac* plane.

Given these trends among the $LnCl_3$ alone, conclusions can be drawn about materials that remain unprobed such as $TmCl_3$. Neighboring both $ErCl_3$ and $YbCl_3$, $TmCl_3$ could exhibit the same in-plane ordering along the *a* axis. However, because thulium is a non-Kramers ion like $TbCl_3$, it could also be an outlier and show ferromagnetic ordering instead of antiferromagnetic ordering. These conclusions are only speculations and thus, must be verified to fill the gap in knowledge. Similar gaps can be found in the $LnBr_3$ and LnI_3 families where the lack of information gives no insight into the trends in magnetic interactions.

4. $LnBr_3$ and LnI_3 Magnetic Structure

Unlike the $LnCl_3$ family, the magnetic orderings and trends of the $LnBr_3$ and LnI_3 families are not well understood. Rather than trends among the same halide family, there appears to be trends among the same lanthanide family LnX_3. Specifically, $CeBr_3$ indicates short range ordering at low temperatures with dominating antiferromagnetic nearest neighbor interactions like $CeCl_3$ [1]. However, the same issue of being unable to fit the linear chain model arises for $CeBr_3$ as well. Arguments for both the linear chain model and xy model are made yet no conclusions could be drawn [9]. Similarly, Krämer reports in-plane antiferromagnetic ordering in both $ErBr_3$ and ErI_3 that mimics $ErCl_3$. However, the materials have an additional short-range ordering in the *c* axis leading to 3D magnetization and stacking disorder [3]. Pistawala reports preliminary results of long range antiferromagnetic ordering of YbI_3 based on magnetization measurements that mimic $YbCl_3$ [21]. Both $YbCl_3$ and YbI_3 indicate a two-step magnetic ordering associated with short range and then long range ordering. However, YbI_3 indicated stronger correlations and crystallizes into the $R\bar{3}$ space group, preserving symmetry compared to that of $YbCl_3$. These examples give insight into the effects of the halide materials on magnetic interactions within the same lanthanide family. Each material acts slightly differently while upholding the same foundational behaviors, shedding light on possible control of these magnetic interactions. However, this in-depth analysis of each LnX_3 family is rarely found and therefore even trends among the same lanthanide trihalide family cannot be made.

$GdBr_3$ and GdI_3 indicate ordering below 1 K, yet no information nor analysis can be found as to what type of ordering occurs [12]. Perhaps they mimic the same ferromagnetic transition as $GdCl_3$ but this conclusion is hard to make without concrete data. Therefore, there is yet another gap in the knowledge on the LnX_3 materials. Unlike the $LnCl_3$ family, the $LnBr_3$ and LnI_3 family has been largely unstudied despite promising evidence that their magnetic interactions can be controlled by changing the halide materials. Though a select few materials have been studied to some degree, many have been left untouched unlike their $LnCl_3$ counterparts. This neglect is once again echoed in the LnOX family despite its attractive van der Waals structure.

B. LnOX

The LnOX family extends the LnX_3 families with the introduction of the oxygen atom, creating 2D structures with weak van der Waals bonds. These materials have been significantly less probed than the LnX_3 family, but their 2D characteristics show strong anisotropy that theoretically could be controlled to effectively realize Kitaev materials. LnOBr materials show characteristic antiferromagnetic signatures at low temperatures in magnetic susceptibility measurements. However, this behavior can only be explicitly seen in SmOBr and DyOBr with crystal field greatly affecting the magnetization of each material [25]. Similar inconclusive results are echoed for GdOCl with magnetic susceptibility: the material shows paramagnetic behavior throughout the measurement, yet the Weiss temperature is -12 K which is indicative of antiferromagnetic behavior [32]. More recently, magnetization measurements of HoOCl, TbOCl, and GdOCl indicate clear antiferromagnetic ordering with Weiss temperatures of <2 K, 3.7 K and 4.8 K respectively [33]. This characterization work fuels a drive to continue exploration into the LnOX family.

DyOCl has shown antiferromagnetic ordering of moments in the *ab* plane and ferromagnetic ordering within a single plane of Dy [34]. These ferromagnetic planes

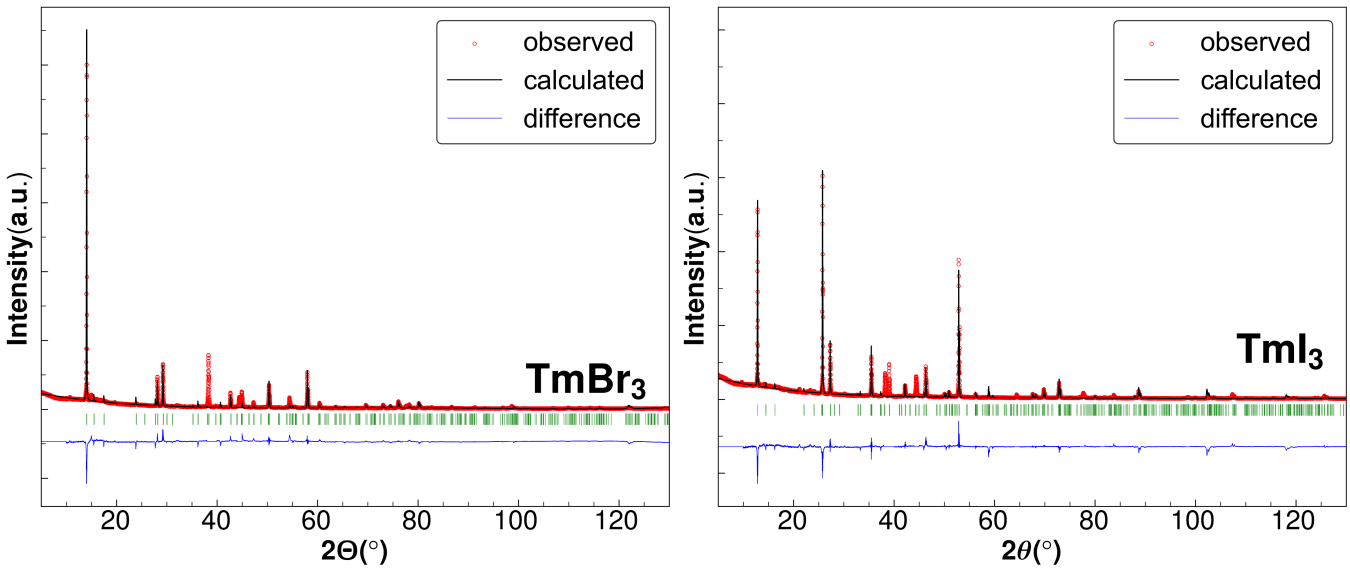

FIG. 1: Powder x-ray diffraction profiles of $TmBr_3$ and TmI_3 (Cu-K_α $\lambda = 1.54$ Å). The red dots are the observed data with the fitted Rietveld refinement profile overlaid using the black line. The residuals are plotted in blue with calculated peak positions appearing as green tick marks beneath the profile. The measurements were taken using air-sensitive sample holders and therefore include aluminum peaks in the diffraction profile. All unfit peaks in the observed profile are aluminum peaks that were masked when conducting the Rietveld refinement.

are stacked antiferromagnetically within the same 2D layer that is quite interesting. Additional reports on this unique behavior of DyOCl indicate there is quadrupolar ordering in the material that is replicated in NdOCl [23]. This behavior is extremely interesting; no compound in the LnX_3 family exhibits quadrupolar ordering. Therefore, the introduction of the oxygen atom could realize similar ordering behavior in other LnOX materials. Once again, since these materials are largely unstudied, it opens the door to finding similar behavior in materials of the same family. For instance, DyOBr and SmOCl indicate antiferromagnetic ordering with DyOBr having strong anisotropy along the a axis and SmOCl along the c axis [35]. Given information on DyOCl and SmOBr, the discrepancy between materials of the same family is indicative of interesting physics at play. The recently proposed Kitaev material YbOCl shows another layer of interesting behavior. Electron spin resonance measurements show a large signal indicative of strong magnetic anisotropy in the ab plane [36]. Even though YbOCl is in the same LnOCl family as DyOCl family, there is no evidence of the quadrupolar ordering. Again, there is evidence of complex interactions affecting the magnetic behavior of these materials, prompting further research into their properties.

In all, 2D LnX_3 and LnOX (X=Cl, Br, I) materials provide the opportunity to observe and theoretically tune magnetic interactions within and between planes of atoms. Though many of these materials have been reported, the TmX_3 and TmOX family has been largely unstudied. Literature on the LnX_3 family focuses on the crystal and magnetic structure of $LnCl_3$ family, all of which seem to follow the UCl_3 structure and 1D linear Ising chain model. Additionally, there is limited information on the crystal and magnetic structure of the $LnBr_3$ and LnI_3 families such that no trends emerged. Literature on the LnOX family carries limited information on their crystal structure, much less their magnetic properties. Other than the preliminary susceptibility measurements on LnOBr and a few deeply studied materials, there is a vast bathe of data that is yet to be collected. Therefore, this project focus on filling the gap in knowledge on the TmX_3 and TmOX materials through x-ray diffraction, magnetic susceptibility, heat capacity, neutron diffraction and neutron scattering measurements. Here, we report on the complete structural and magnetic characterization of $TmBr_3$ and TmI_3 as well as the partial characterization of TmOBr.

III. METHODS

Polycrystalline samples of $TmBr_3$ and TmI_3 were commercially purchased from Alfa Aesar at 99.99% purity. Polycrystalline TmOBr was synthesized using a nitrogen tube furnace and solid state synthesis. Details about the exact synthesis methods can be found in Section A of the Supplementary Information. Due the hygroscopic nature of all materials, all handling of the samples was done in a glovebox under an inert argon atmosphere. The phase purity of each sample was confirmed with powder x-ray diffraction (PXRD) using a Rigaku Smartlab SE (Cu-K_α

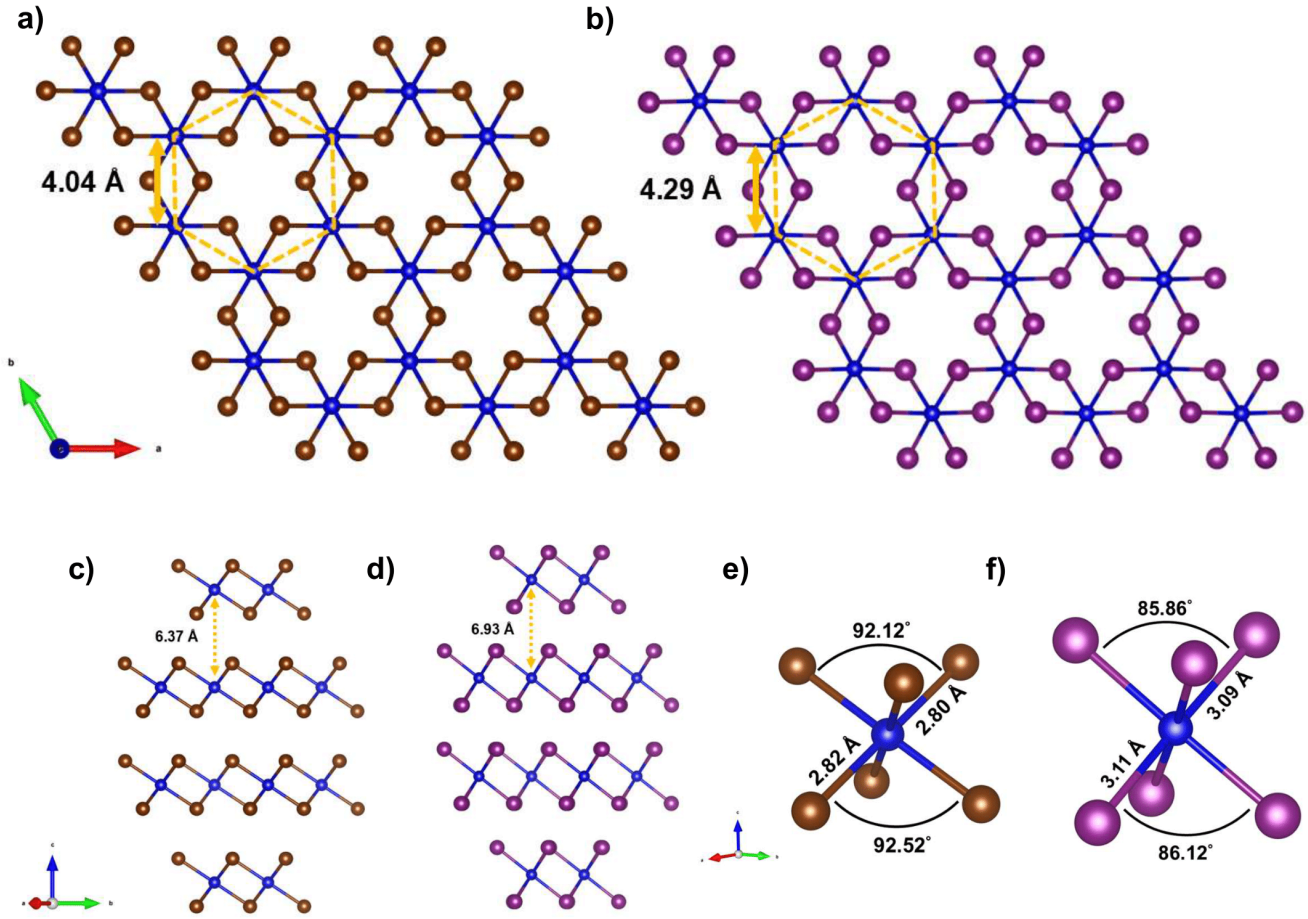

FIG. 2: The proposed crystal structure of $TmBr_3$ and TmI_3 as determined from the powder XRD Rietveld refinements. a) A single layer of $TmBr_3$ viewed along the c axis. The thulium atoms (blue dots) are arranged in a symmetrical hexagonal system bonded by bromine atoms (brown dots) and separated by a distance of 4.04 Å. b) A single layer of $TmBr_3$ viewed along the c axis. The thulium atoms (blue dots) are arranged in a symmetrical hexagonal system bonded by iodine atoms (purple dots) and separated by a distance of 4.29 Å. c) A single unit cell of $TmBr_3$ in standard orientation. Each layer contains thulium atoms bonded to bromine atoms. Each layer is van der Waals bonded to the next, maintaining an interlayer Tm-Tm distance of 6.37 Å. d) A single unit cell of TmI_3 in standard orientation with an interlayer Tm-Tm distance of 6.37 Å. e) The environment of a single thulium atom in $TmBr_3$. Each atom has three Tm-Br 2.80 Å bonds and three 2.82 Å bonds that alternate their vertical position along the ab plane of each layer. The difference in bond lengths results in different Br-Tm-Br bond angles of 92.12 degrees and 92.52 degrees. f) The environment of a single thulium atom in TmI_3. Each atom has three Tm-I 3.11 Å bonds and three 3.09 Å bonds with I-Tm-I bond angles of 85.86 degrees and 86.12 degrees respectively.

$\lambda = 1.54$ Å) and air sensitive sample holders. Rietveld refinement was done using Fullprof after phase purity was confirmed to identify the space group, lattice parameters, and atomic positions [37].

Temperature dependent and isothermal magnetization measurements were done using the Physical Property Measurement System (PPMS) from Quantum Design. For temperature dependent magnetization, two sets of measurements were done from 300 to 1.8 K (zero field cooling) and from 1.8 K to 300 K (field cooling). Zero field cooling data was used to extract the Weiss temperature and effective moment as both datasets look similar as seen in Figure S2 in the Supplementary Information. The normalized, inverse data was fit to the inverse Curie-Weiss law $\chi^{-1}(T) \approx \frac{8}{\mu_{\text{eff}}^2}(T - \theta_{CW})$ where μ_{eff} is the effective moment and θ_{CW} is the Weiss temperature. These fits were done as a function of temperature ranges to ac-

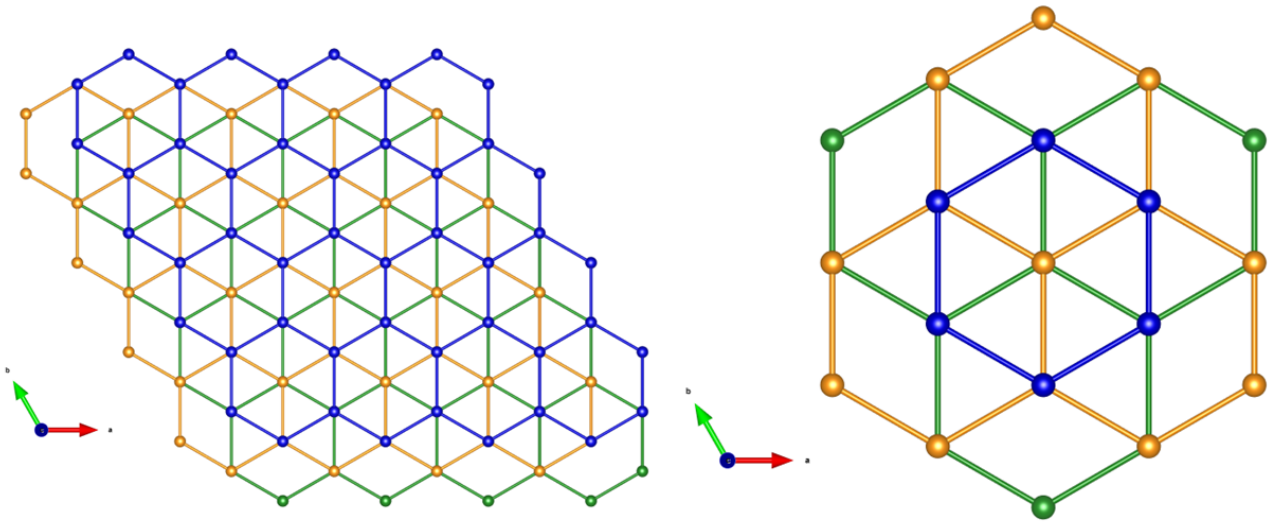

FIG. 3: A top down view of the symmetrical hexagonal system of thulium atoms in $TmBr_3$ and TmI_3 as determined from the powder XRD Rietveld refinements. The Tm-Tm bonds are for visualization of the hexagonal system only and do not actually exist, showing nearest neighbor and next nearest neighbor interactions. The atomic layers appear to go into the page, with blue dots representing the top most layer, yellow dots representing the layer behind it, and green dots representing the very last layer. Each layer of Tm atoms does not line up with the one below it, creating a complex pattern of interactions.

count for possible deviations from the Curie-Weiss law. More information about fitting ranges and resulting parameters can be found in Figure S3 in the Supplementary Information. The effective g factor was calculated using the equation $\mu_{\text{eff}} = g_{\text{eff}}^2 J(J+1)$ and assuming the effective J value is 1. Isothermal magnetization was fit at high fields to extract the magnetic saturation value m_s and subsequently the effective g factor using the equation $m_s = g_{\text{eff}} J$. Magnetic saturation m_s was compared to the effective moment to identify if the system was Ising-like or Heisenberg-like. All fitting was done using original Python scripts.

Using the dilution refrigerator from QuantumDesign, heat capacity measurements were conducted from 50 mK to 300 K on the PPMS as well. To prevent degradation of the samples when mounting, a mound of N grease was added to the sample mount for the addenda measurements. The polycrystalline samples were pressed into flakes using a hand press in the glovebox. Appropriate flakes were mounted onto the sample holder and subsequently covered in the excess N grease. The resulting data (C_{P}/T vs T) was fit to the triple Debye model to subtract thermal vibrations at high temperature and the reduced data was fit to $y = \alpha T^{-3}$ at low temperature to account for nuclear Schottky contributions. The magnetic heat capacity was integrated and fit to $S = k_b \ln\Omega$ to identify the change in entropy as a function of temperature.

Neutron powder diffraction measurements were done on HB2A at the High Flux Isotope Reactor (HFIR) at Oak Ridge National Laboratory (ORNL). Powder samples of $TmBr_3$ and TmI_3 were specially mounted into ~15 mm aluminum cans due to their high neutron absorption. Roughly two grams of each powder was evenly spread onto half of a 5x7 cm sheet of aluminum foil. The sheet was folded in half and the edges were folded to create a sealed foil envelope. The envelope was then rolled around a vial to form a hollow cylinder shape, allowing the powder sample to sit on the walls of the aluminum can. Each aluminum can was sealed under 1 atmosphere pressure of ^{4}He to prevent oxidation in air and provide an exchange gas during the measurement. Measurements were conducted at temperatures of 0.27, 1.7, 4, and 50 Kelvin on the sample cans to observe diffraction below magnetic ordering, above ordering temperature, magnetic diffuse scattering, and at high temperature respectively. An empty can was measured at 0.27, 1.7, and 50 K to account for background noise. All measurements

between 0.27-4 K were done using a wavelength of 2.41 Å while high temperature data at 50 K was done using a wavelength of 1.54 Å.

Inelastic neutron scattering measurements were done on the MARI instrument at the ISIS Neutron and Muon Source. Measurements were done at 5 and 150 K for $TmBr_3$ and at 5, 50, and 150 K for TmI_3 to capture low temperature and high temperature crystal field excitations. Incident neutron energy was set to 180 meV with repetition-rate multiplication (RRM) allowing energies of 29.7 meV and 11.7 meV at a chopper frequency of 400 Hz for both samples of $TmBr_3$ and TmI_3. Roughly 6.7 g of $TmBr_3$ and 5.5 g of TmI_3 powder were prepared for the measurements using the same aluminum can methods as the neutron powder diffraction. The scattering profiles were plotted using MANTID software and fit with PyCrystalField to understand the crystal field splittings and Hamiltonian of the systems.

IV. RESULTS

A. Crystal Structure

The observed and calculated powder x-ray diffraction patterns for $TmBr_3$ and TmI_3 are shown in Figure 1. The profile was refined in the known trigonal space group $R\bar{3}$ (No. 148). The powder x-ray diffraction pattern for both materials indicates significant preferred orientation along the c axis with the most significant peaks corresponding to the (003), (006), and (0012) *hkl* lattice planes. Therefore, to obtain a good refinement, preferred orientation along the (003) *hkl* plane was introduced and the aluminum peaks from the sample holder were masked. Peaks that appear to not have a calculated profile in Figure 1 are the masked aluminum peaks. The results of the refinement for $TmBr_3$ and TmI_3 respectively can be found in Table II. The observed powder x-ray diffraction pattern for TmOBr is shown in Figure S1 in Supplementary Information. Preliminary analysis of the profile indicates the material crystallizes into the space group P4/nmm (No. 129) with little impurities. Further work is needed to refine the lattice parameters and atomic positions.

Figure 2 illustrates the hexagonal crystal structures of $TmBr_3$ and TmI_3. As seen in Figure 2a and Figure 2b, the Tm atoms are arranged in a symmetrical hexagonal system with each Tm atom sharing two halide atoms with its nearest neighbor. The intraplanar Tm-Tm distance is different between the materials due to different halides, with $TmBr_3$ at 4.04 Å and TmI_3 at 4.29 Å. Similar differences in atomic distances between the materials can be seen in Figure 2c and 2d. The materials consist of quasi 2D planes of thulium and halide atoms that are van der Waals bonded together. The interplanar Tm-Tm distance is 6.37 Å for $TmBr_3$ and 6.93 Å for TmI_3. Figure 2e and 2f illustrates the crystal environment of a single thulium atom in $TmBr_3$ and TmI_3 respectively. Each thulium atom is bonded to six halide atoms, creating a near perfect octahedral environment. The halide atoms are split such that three halide atoms are bonded equidistantly above the Tm atom and three halide atoms are bonded equidistantly below the atom. Within each plane, the different bond lengths alternate to prevent planar canting. Additionally, this difference in bond lengths results in two different X-Tm-X bond angles. $TmBr_3$ has bond lengths of 2.80 and 2.82 Å while TmI_3 has bond lengths of 3.09 and 3.11 Å. The difference in roughly 0.2 Å could be inferred to be within error bars, explaining the phenomena that occur in other measurements. However, further work is needed to completely rule out the possibility of error in the refinement.

The symmetrical hexagonal system of thulium atoms can be seen clearly in Figure 3. It is important to note the Tm-Tm bonds are strictly for visualization purposes and do not chemically exist in the structure of the materials. Viewed along the c axis, each color represents a thulium atom on a different plane in the following sequence from the bottom up: green at the base, yellow in the middle, and blue on top. Focusing on one hexagonal system of blue atoms, the two layers below are vertically misaligned in a symmetric fashion. The misaligned unit cell contains three layers of thulium atoms, introducing the possibility of staggered interlayer interactions dominating intralayer interactions.

Parameters	$TmBr_3$	TmI_3
a (Å)	6.999779	7.425272
b (Å)	6.999779	7.425272
c (Å)	19.100077	20.781199
α (°)	90.00	90.00
β (°)	90.00	90.00
γ (°)	120.00	120.00
Tm Position x	0	0
Tm Position y	0	0
Tm Position z	0.33339	0.33333
Halide Position x	0.33478	0.32440
Halide Position y	0.33089	0.33474
Halide Position z	0.41485	0.42525

TABLE II: Refined crystal lattice parameters and atomic positions of $TmBr_3$ and TmI_3.

B. Magnetization

Inverse magnetic susceptibility $\chi^{-1}(T)$ for all three materials can be seen in Figure 4. Based on the fitting analysis, $TmBr_3$ has a Weiss temperature of -0.3 K, μ_{eff} =7.5 μ_B, and g_{eff} = 5.3 while TmI_3 has a Weiss temperature of -4.9 K, μ_{eff} = 7.7 μ_B, and g_{eff} = 5.4. TmOBr has a Weiss temperature of -21.5 K, μ_{eff} = 7.6 μ_B, and g_{eff} = 5.3. As seen in Figure 4, the materials appear to follow the paramagnetic regime throughout the entire temperature range of the measurement as there is very little devi-

ation from the inverse Curie-Weiss law. However, below 50 K, there are slight deviations indicative of a different magnetic regime. These deviations are predicted to be antiferromagnetic in nature as indicated by the negative Weiss temperatures of -0.3, -4.9, and -21.5 Kelvin for $TmBr_3$, TmI_3, and TmOBr respectively. It is important to note the close proximity of $TmBr_3$'s Weiss temperature to zero as an indication of either no interactions or strong competing interactions. These interactions could lead to the absence of magnetic order at very low temperatures and potential spin liquid candidacy. Additionally, the effective moment from $TmBr_3$, TmI_3, and TmOBr differ from the Tm^{+3} free ion magnetic moment of 7.56 μ_B, indicating crystal field effects are at play.

Isothermal magnetization at 1.8 K for all three samples are shown in Figure 5. As seen, $TmBr_3$ shows slight saturation around 7 Tesla whereas TmI_3 does not saturate until roughly 10 Tesla. On the other hand, TmOBr appears to reach saturation around 4 Tesla yet continues to increase in magnetization. The absence of complete magnetic saturation is another indication that crystal field effects are at play. Fitting at high fields results in magnetic saturation values of 2.884 μ_B, 2.812 μ_B, and 3.228 μ_B for $TmBr_3$, TmI_3, and TmOBr respectively. Resulting g factor analysis indicates $g_{\text{eff}} = 2.88$ for $TmBr_3$, $g_{\text{eff}} = 2.81$ for TmI_3, and $g_{\text{eff}} = 3.22$ for TmOBr. Lastly, this effective g factor from the isothermal calculation was divided by the effective g factor calculated from the fitted effective moment to get a scale factor X. For $TmBr_3$, this factor is 0.545, for TmI_3 it is 0.516, and for TmOBr it is 0.604. Qualitatively, due to powder averaging, this value indicates an Ising like system if close to 0.5 and a Heisenberg or XY like system if anything else. Using this logic, $TmBr_3$, TmI_3, and TmOBr can be qualitatively determined to be a more Ising like systems. However, this analysis is incomplete without considering the magnetic diffraction data, the true indicator of the magnetic structure of both materials.

C. Heat Capacity

Low temperature heat capacity curves are shown in Figure 6. $TmBr_3$, TmI_3, and TmOBr all show magnetic ordering between 1 and 2 Kelvin. Specifically, magnetic ordering in $TmBr_3$ requires 4 Tesla of applied magnetic field to completely diminish compared to TmI_3 that requires less than 1 Tesla. This is another piece of evidence indicating strong competing interactions rather than no interactions in $TmBr_3$ compared to TmI_3. Similarly, TmOBr requires 4 Tesla of applied magnetic field to diminishes the magnetic ordering peak with no signatures of a nuclear contribution at low temperature. Instead, there is an anomalous peak around 0.2 K under an applied field of 1 Tesla that appears in addition to the magnetic ordering peak around 1 K. Further work is needed to confirm if this peak is the onset of additional magnetic phenomena from the sample or from impuri-

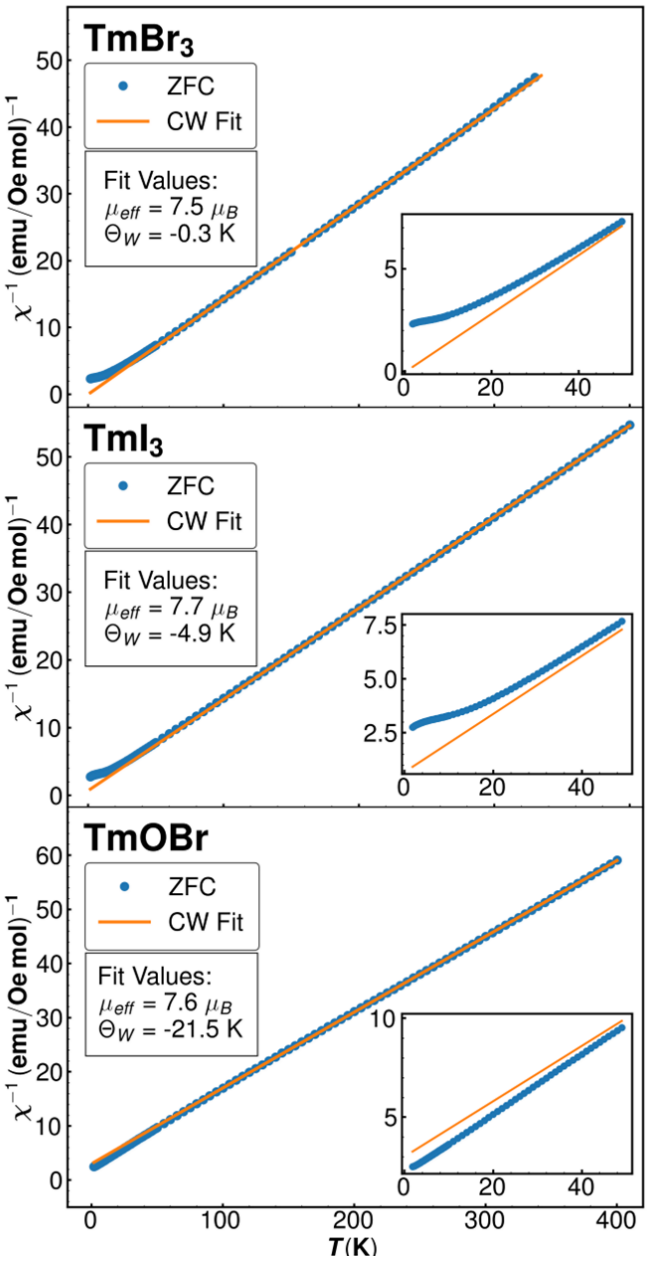

FIG. 4: $TmBr_3$, TmI_3, and TmOBr inverse magnetic susceptibility (blue dots) as a function of temperature with the Curie-Weiss fit (orange line) overlaid. Data was taken on the temperature range of [1.8, 350 K] for $TmBr_3$ and [1.8, 400 K] for TmI_3 and TmOBr with slight deviations from the Curie-Weiss law visible below 50 K. Subsequent data was fit as a function of the temperature range to extract the effective moment and Weiss temperatures and reduce errors in the fitted values. Fit values based on temperature range can be found in Figure S3 in the Supplementary Information. Measurement error bars are too small to be visible on the plot. Inset: Zero field cooled data (ZFC) and the Curie-Weiss fit below 50 K. Both materials show a deviation from the Curie-Weiss law indicating the onset of correlations.

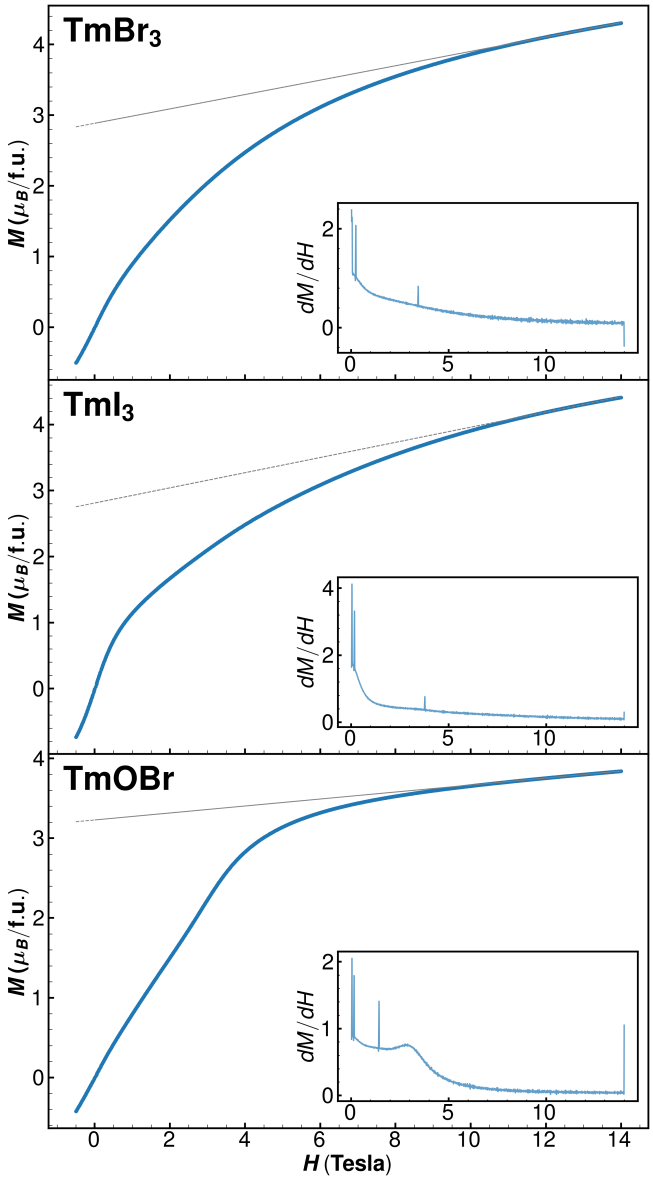

FIG. 5: Isothermal magnetization of $TmBr_3$, TmI_3, and TmOBr at 1.8 K as a function of applied magnetic field on the range of [0,14 T]. Magnetization for $TmBr_3$ and TmI_3 materials does not achieve clear saturation within the measurement range. A linear fit was performed for all materials at high field range of [12, 14 T] and extrapolated to zero field to extract a magnetic saturation value m_s. Magnetic saturation occurs at 2.884 μ_B for $TmBr_3$, at 2.812 μ_B for TmI_3, and at 3.228 μ_B for TmOBr . Inset: The derivative of magnetization as a function of applied magnetic field. All the derivatives do not completely diminish, indicating the need of a higher magnetic field to achieve magnetic saturation. Spikes in the derivative data arise from gaps in the measurement, a consequence of equipment blips during the measurement.

ties/errors in the measurement.

The heat capacity data for TmI_3 on the temperature range of [0.05, 10 K] can be seen in Figure 7. The data shows an upturn below and above the phase transition peak due to nuclear and phonon contribution respectively. Phonon contribution was captured with a triple Debye model fitted on the temperature range of [10, 200 K], avoiding the sample phase transition peak at low temperature and grease phase transition at 250 K. The error-based weighted fit yielded Debye temperatures of 64.18, 218.34, 794.24 Kelvin, ruling out the possibility of phonon contribution in the observed peak. The nuclear contribution was approximated using the equation $y = \alpha T^{-3}$ to capture the high temperature tail of the Schottky anomaly closest to 0 Kelvin. At this point, it is unclear if the second peak between the Schottky anomaly and phase transition is a secondary magnetic transition or a primary nuclear contribution. Nevertheless, it is clear that the magnetic phase transition signature is very small compared to the nuclear and phonon contribution.

This is more apparent in the magnetic and nuclear entropy plot in Figure 8 where, despite including the nuclear contribution in the entropy calculations, the entropy of the system saturates at 4.2 % of Rln2. This entropy is a very small number compared to YbI_3 and could be a unique characteristic of the non-Kramers ion thulium [21]. The heat capacity of $TmBr_3$ and TmI_3 in Figure 6 have characteristically low signal strengths despite the presence of a phase transition peak. As reported by Pistawala, the single crystal YbI_3 has a phase transition peak intensity of roughly 2.5 $JK^{-2}mol^{-1}$ compared to the 0.2 $JK^{-2}mol^{-1}$ of TmI_3 [21]. This severe mismatch could be attributed to differences between powder and single crystal samples, yet heat capacity measurements were conducted multiple times at various different times for TmI_3. Each data set produced similar results, indicating some collective phenomena could be at play. Further analysis is required to complete parse the entropy results and investigate the secondary peak at 0.3 K before reaching any conclusions. Further data collection is required at high temperature for $TmBr_3$ and TmOBr to investigate if the low entropy release is unique to thulium compounds.

D. Magnetic Structure

1. *Crystal Field Excitations*

Inelastic neutron scattering profiles at 5 Kelvin of $TmBr_3$ and TmI_3 can be seen in Figure 9. The elastic mode is represented by the brightly populated line at 0 meV in all plots, with the remaining signal strength attributed to populated crystal field modes and magnetic excitations. At E_i =180 meV, there is an absence of crystal field modes that is quite evident given the very low intensity of 0.2 used to display the energy modes. At incident energies of 11.7 and 29.7 meV, both $TmBr_3$ and

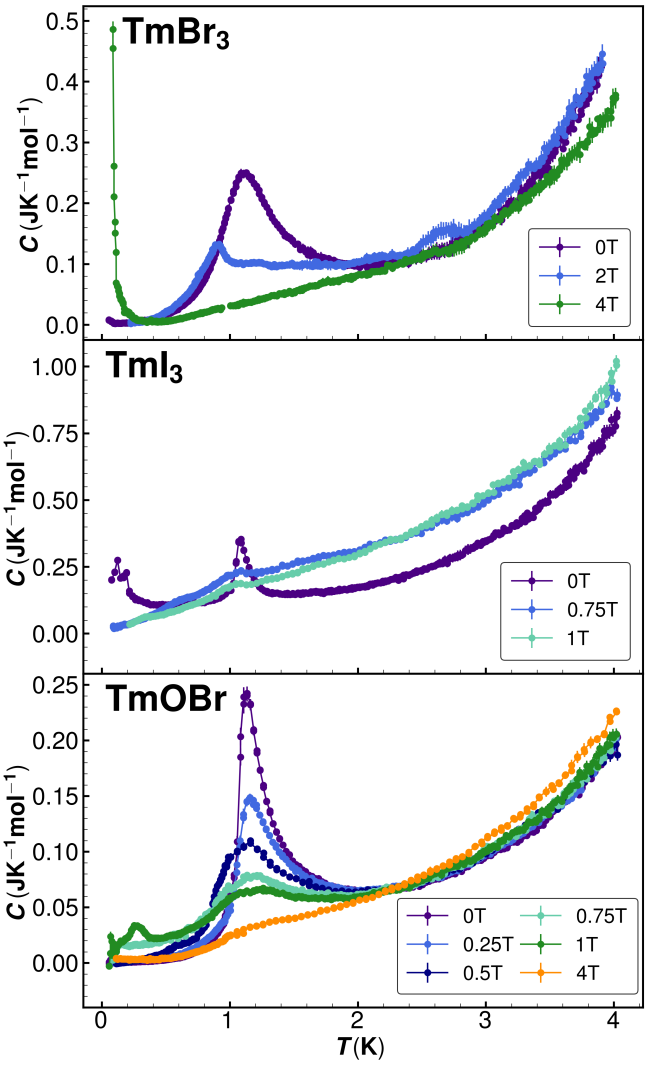

FIG. 6: Low temperature heat capacity of both materials measured at various applied magnetic fields. The upturn near 4 K in all data sets is attributed to phonon contribution while the upturn near 0 K in all data sets is attributed to the nuclear Schottky contribution. All samples showcase a phase transition that is believed to be magnetic in origin just above 1 Kelvin. It is important to not the absence of the nuclear contribution in TmOBr but the emergence of a peak around 0.2 K under an applied magnetic field of 1 Tesla.

TmI_3 display neutron-excited crystal field modes around 7.9 meV and 4.1 meV respectively. Both modes are flat across momentum space under different energies, a clear indication of a crystal field mode. The absence of other crystal field modes could be a result of accidental degeneracy points. Assuming octahedral symmetry for the thulium environment, the single-ion modes often cross and lead to accidental degeneracy points where high energy crystal field modes are absent [38]. Further analysis of the crystal field modes is required to extract the system's Hamiltonian and determine the presence of an accidental degeneracy.

The signal in $TmBr_3$ at 2.5 meV is possibly not a crystal field mode but rather a magnetic excitation. As seen in the $E_i = 11.7$ meV plot of Figure 9, there is a slight downturn in the mode from the plot edge followed by an upturn around $|Q| = 2$ Å^{-1}. Although subtle, this dispersion is mimicked in the 29.7 meV plot with the same line shape occurring at the same locations in momentum space. The presence of this low lying magnetic excitation in $TmBr_3$ could be a result of strong competing interactions between the nearest neighbor and next nearest neighbor magnetic ions. Though mere speculation, coupled with low Weiss temperature of -0.3 Kelvin, $TmBr_3$ could potentially host both ferromagnetic and antiferromagnetic ordering. However, further analysis of these results is needed to support this conclusion.

2. *Magnetic Diffraction*

Neutron diffraction profiles for both samples done at 0.27 K and 4 K can be seen in Figure 10. Because the measurements were done in aluminum cans and foil, many of the major peaks appearing in the diffraction profile can be attributed to aluminum. Figure 11 shows the magnified diffraction profiles at 0.25 K and 4 K for both

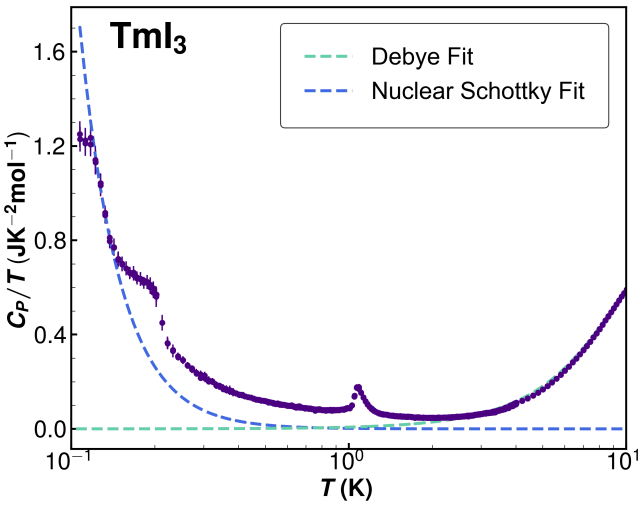

FIG. 7: Zero field heat capacity over temperature as a function of temperature (purple dots). The phonon contribution was approximated using a error-based weighted triple Debye model (teal dashed line) fitted to the temperature range [10, 200], resulting in Debye temperatures of 64.18, 218.34, 794.24 Kelvin. The high temperature tail of the nuclear Schottky anomaly (blue dashed line) was approximated using the equation $y = \alpha T^{-3}$ and fitted to temperatures below the phase transition peak.

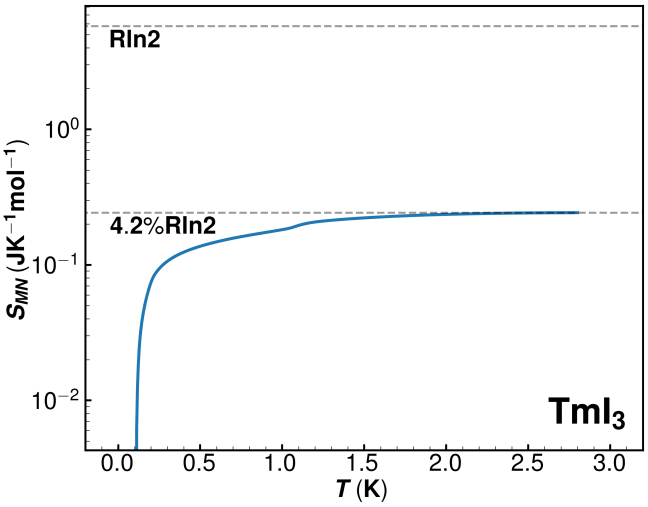

FIG. 8: Magnetic and nuclear entropy as a function of temperature plotted with the Rln2 threshold. Integration was done to 3 K in temperature after the phonon contribution was subtracted from the data. The entropy of they system reaches a threshold that is 4.2 % of Rln2.

samples plotted with the difference between the two profiles. As seen, there are two very weak magnetic Bragg peaks in $TmBr_3$ around 26 and 32 degrees below magnetic ordering temperature. Additionally, an even weaker peak can be seen for TmI_3 around 30 degrees. Further work is needed to be done to completely understand the magnetic structure and propogation vector.

V. DISCUSSION

As shown, the structural and magnetic behavior of $TmBr_3$, TmI_3, and TmOBr is similar yet different. For the sake of clarity, the following discussion is divided to individually discuss the materials before comparing $TmBr_3$ and TmI_3 to each other and current literature.

A. $TmBr_3$

The behavior of $TmBr_3$ is rather complex compared to its siblings in the TmX_3 family. Crystallizing into the $R\bar{3}$ space group, the c axis lattice parameter is drastically different between the high temperature x-ray diffraction data at 300 K and the high temperature neutron powder diffraction data done at 50 K. Though both are somewhat close, 19.1 and 18.85 Å repectively, refinements indicate decreasing the temperature decreases the interplanar distances. This is rather uncommon as the Yb counterpart shows no such behavior [16]. The data and refinement themselves could be attributed to the discrepancies between the similar materials, however, it is not entirely uncommon to see shifts in crystal structure with temperature. $YbCl_3$ transforms space groups at low temperatures due to the lack of phonon vibrations present at high temperatures [21]. Though the change in $TmBr_3$ is not as drastic as changing space groups, differences in the c axis could be a result of relaxing phonon vibrations and interactions.

Magnetically, $TmBr_3$ appears to be the most complex. As seen from the magnetic susceptibility and isothermal magnetization, the Curie-Weiss temperature is very close to zero and there is a lack of magnetic saturation reached. This indication of strong competing interactions persists in the heat capacity as well. There, the magnetic ordering peak around 1 Kelvin takes a high applied field of 4 Tesla to completely vanish. Inelastic neutron scattering and elastic scattering reflect similar results. One populated ground state energy mode indicates a strong influence of the crystal field on the magnetic interactions and a possible magnetic excitation wave hints there is more at play. This is once again reflected in the magnetic diffraction peaks where there are two significant Bragg peak. Analysis of both of these features indicates the magnetic structure of $TmBr_3$ is rather complicated.

Specifically, from the magnetization data, the system must be Ising; therefore we can eliminate non-collinear potential ground states, yet there are still many to consider. Inelastic scattering showcases one low energy mode corresponding to the crystal electric field splitting and a possible low energy magnetic excitation. These results implies the potential magnetic ground state is characterized by weak interplanar ordering and strong intraplanar ordering. This conclusion is particularly interesting compared to its Yb and Er counterparts [3, 16]. Though neither of the materials have conclusive magnetic structures, they indicate that thulium should have interplanar antiferromagnetic ordering with next nearest neighbor exchanges dominating near neighbor ones. Further work is needed to truly conclusively define the magnetic ground state of $TmBr_3$, including magnetic structural refinements and crystal field fitting.

B. TmI_3

TmI_3 appears to be the most simple in its crystal structure and its magnetic properties. The lattice parameters are consistent throughout various temperature regimes, indicating the phonon vibrations and lattice distortions are either non-existent or at an energy scale that does not affect the overall crystal structure. Similarities can be found with the Yb and Er counterparts that do not change space groups or lattice parameters at low temperatures [3, 21].

Magnetically, the material appears to have an antiferromagnetic regime at low temperature as indicated by the negative Weiss temperature of -4.9 Kelvin. Though this number is not quite as close to zero, there could be some competing interactions at play. This is replicated

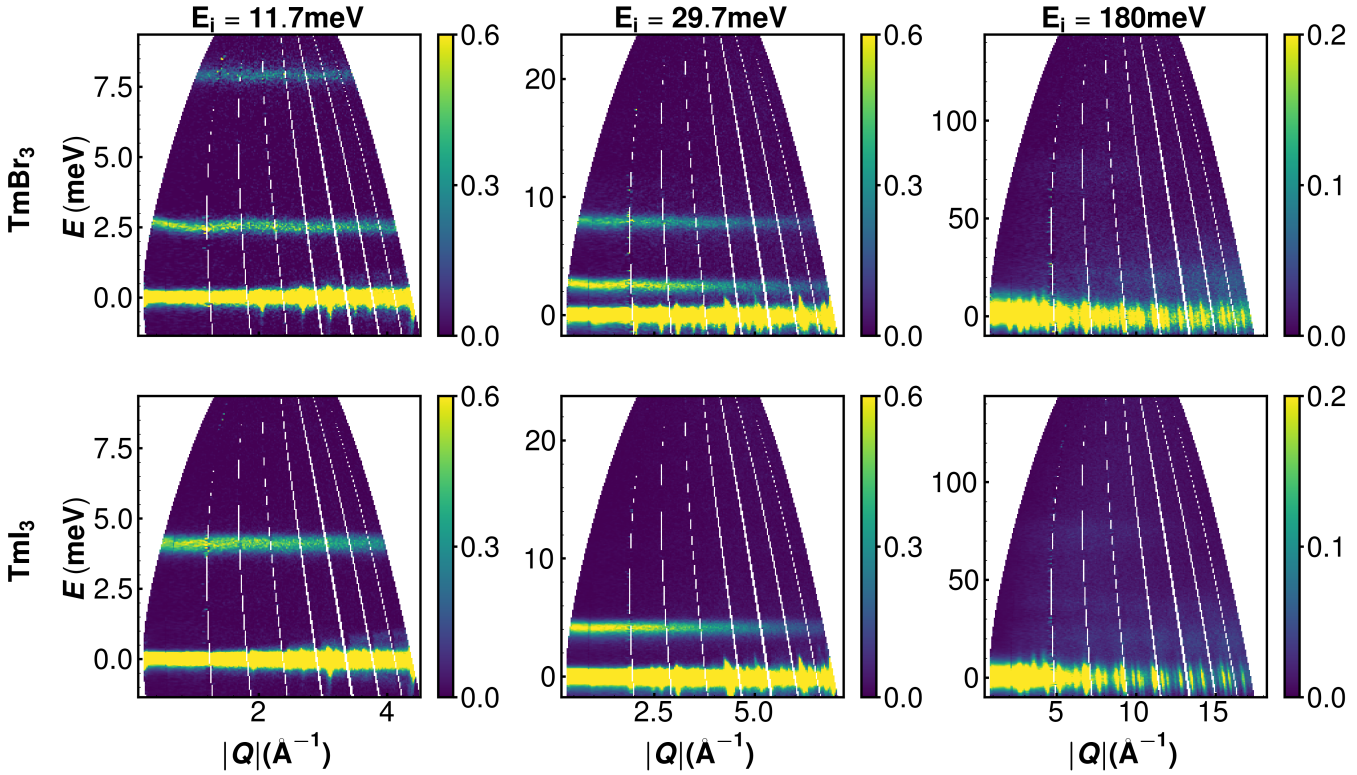

FIG. 9: Powder inelastic neutron scattering plots of $TmBr_3$ and TmI_3 taken at three incident energies of 11.7, 29.7, and 180 meV at 5 Kelvin. All elastic scattering is captured and plotted as the bright line at 0 meV. Top row: $TmBr_3$ showcases two distinct energy signals at 2.5 and 7.9 meV under incident energy of 11.7 and 29.7 meV. The higher energy signal at 7.9 meV is attributed to a low lying crystal field mode while the lower energy signal at 2.5 meV is attributed to a magnetic excitation. Bottom row: TmI_3 showcases only one low lying crystal field mode at 4.1 meV under incident energy of 11.7 and 29.7. The $E_i = 180$ meV confirms the absences of high energy crystal field modes in both materials.

in the isothermal magnetization where there seems to be saturation around 2 Tesla of applied field; however, the magnetization continues to increase without reaching a plateau. This is particularly interesting given the Er and Yb counterparts both show magnetic saturation around 12 Tesla [3, 21]. This phenomena could be an implication of a non-Kramers doublet ion introducing crystal field effects that prevent saturation. On the other hand, this result could be the effect of using a powder sample in magnetization measurements. For instance, perhaps the sample used was not completely ground together, causing large chunks of sample to not see the full magnitude of the applied field. Another measurement needs to be conducted to corroborate the latter theory. Heat capacity measurements indicate the sample magnetically orders around 1 Kelvin as expected, with the peak diminishing under an applied field of 1 Tesla. This is evidence that either the magnetization or the heat capacity measurement was not conducted properly as the low applied field indicates the competing interactions are not strong.

The magnetic structure also shows rather simple interactions between the magnetic dipoles. The inelastic scattering indicates only one crystal field energy mode at very low temperatures and energies with no magnetic excitations. This indicates the crystal field effects are minimized for this compound due to the larger distances between interplanar and intraplanar magnetic dipoles. Magnetic diffraction also shows a very weak peak that gives rather ambiguous magnetic structures. From the magnetization data, the system must be Ising, therefore we can eliminate canted ground states, yet there are still many to consider. Inelastic scattering showcases only one low energy mode corresponding to the crystal electric field splitting. Therefore, it is difficult to eliminate any potential ground states. Lastly, entropy calculations indicate 4.2 percent of entropy is gained from the magnetic transition, a rather anomalous result. The exact nature of the ground state needs further analysis in relation to its Br counterpart given the higher number of potential ground states. Similar conclusions have been reached in TmI_3's Yb and Er counterparts, where neither materials have conclusive magnetic structures [3, 21]. This could be the effect of the non-Kramers ion with an effective singlet ground state configuration or the effect of the iodide. Iodine has a large ionic radius, forcing the nearest neighbor and next nearest neighbor interactions to be

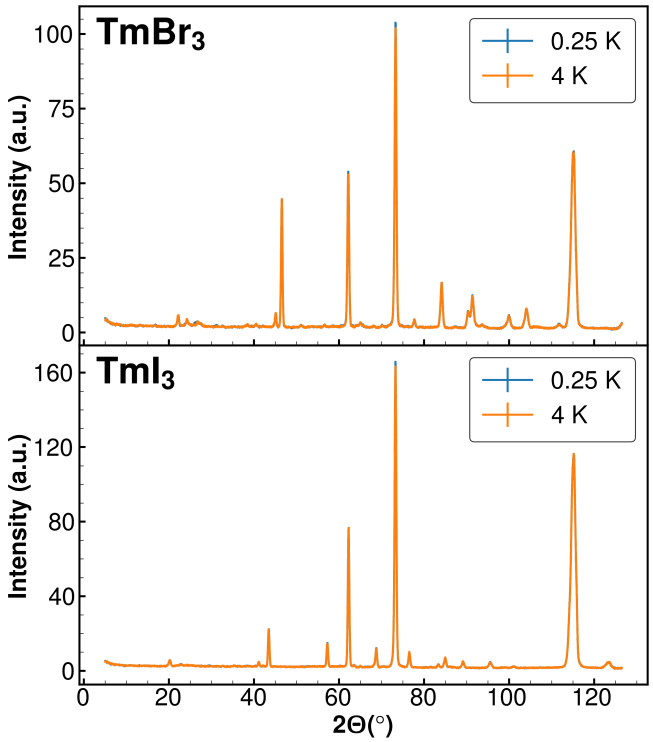

FIG. 10: Powder neutron diffraction profiles of $TmBr_3$ and TmI_3 taken with $\lambda = 2.41$ Å. Measurements were taken at 0.25 K (blue dots) and 4 K (orange dots) to capture magnetic Bragg peaks below and above the ordering temperatures respectively. The profiles show subtle differences, with the weak magnetic Bragg peaks more clearly portrayed in Figure 11. Aluminum sample cans appear in the diffraction profiles as the most intense peaks.

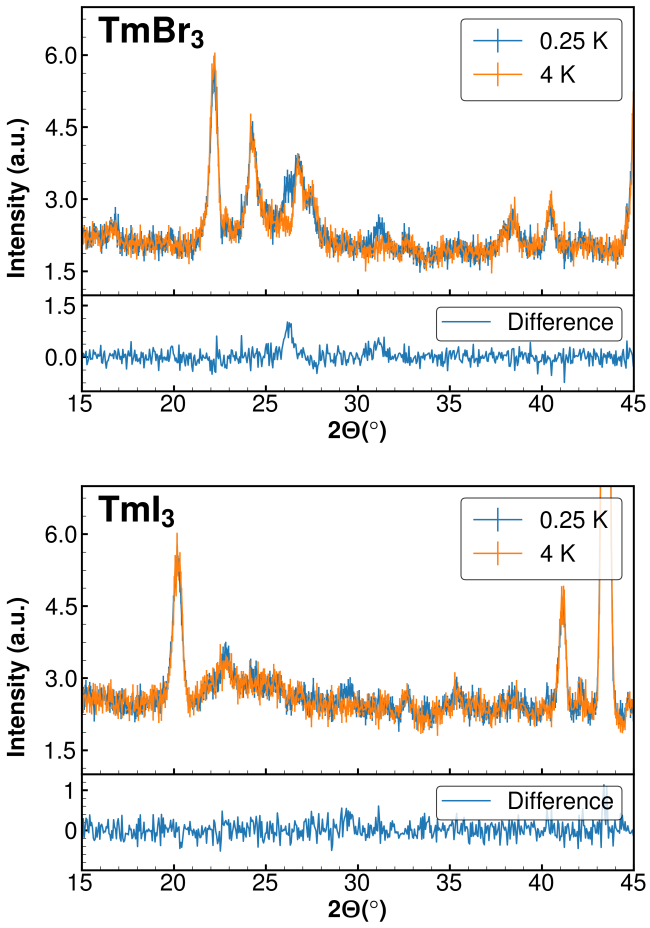

FIG. 11: A zoomed in view of the neutron powder diffraction profiles of $TmBr_3$ and TmI_3 taken at 0.25 K and 4 K and the difference in profiles. In both materials, there are very weak magnetic Bragg peaks in the scattering angle range [25°, 35°] as seen by the differences in the 0.25 K and 4 K profiles. $TmBr_3$ shows two magnetic Bragg peaks around 26 and 32 degrees in both the overlaid plot and the subtracted plot. TmI_3 shows a much weaker magnetic Bragg peak just before 30 degrees that is hard to discern in the difference plot.

further than the bromine counterpart. In theory, this increased distance isolates the magnetic dipole and allows for magnetic ordering and lower energy modes. However, because the materials is at a low energy scale, there is less conclusive evidence to determine the magnetic ground state. Further analysis is needed to understand the exact magnetic structure and crystal field Hamiltonian of TmI_3 in comparison to $TmBr_3$.

C. TmOBr

TmOBr presents similar yet interesting results in comparison to $TmBr_3$ and TmI_3. Though the structural analysis is incomplete, the powder sample used throughout the measurements appears to be crystalline and belongs to the P4/nmm space group. This preliminary analysis echoes the results from literature, where Hölsä reports the same [25]. Magnetically, the material appears to have an antiferromagnetic signature at low temperature as indicated by the negative Weiss temperature of -21.5 Kelvin, similar to the -23.8 as reported by Hölsa [25]. Isothermal magnetization indicates TmOBr begins the reach magnetic saturation around 4 Tesla, yet continues to increase at a very slow rate. Similar to $TmBr_3$ and TmI_3, the qualitative analysis of the effective g factor ratios indicates TmOBr is an Ising-like system. Perhaps the magnetic structure of TmOBr is dictated by Kitaev physics similar to those present in YbOCl, where the system is dominated by anisotropic coupling [36]. However, this is mere speculation and further work — neutron diffraction and scattering measurements — needs to be done to truly identify the magnetic interactions in TmOBr.

The notable magnetic feature present in TmOBr is the anomalous peak at 0.2 K under an applied magnetic field of 1 Tesla. Observed data taken at applied

field ranges of [0, 0.75 T] show expected behavior: the emergence of a phase transition peak is diminished with applied field, with no nuclear contribution present within the measured temperature range. The migration of the peak position as a function of applied field indicates the transition is magnetic in nature. At a high applied field of 4 Tesla, the peak vanishes as expected. Only in the 1 Tesla data is their an emergence of a secondary peak around 0.2 Kelvin. Possible explanations to this phenomena include experimental error during measurement where an impurity materialized due to the long measurement time. It could also be attributed to a technical error with the equipment at that specific applied field. This argument, however, is not as substantial as sample impurities. Measurements taken on three separate occasions using separate phase pure samples indicate the same results. Rather than impurities or clerical errors, this anomaly could be attributed to the onset of magnetic behavior. Further measurements are needed at various intermediate applied fields to distinguish the onset of such phenomena.

D. $TmBr_3$ vs. TmI_3

Despite similar crystal structures between the two materials, there are drastically different magnetic behaviors. As established before, both materials crystallize into the $R\bar{3}$ (No.148) space group. Changing the halide material from bromine to iodine changes the lattice parameters as expected, an increase in both the a and c axes. The space group allows for quasi two dimensional planes that are bonded together with weak van der Waals bonds, similar to the behavior of its Yb analog [16, 21]. Despite these changing lattice parameters, the J_1 nearest neighbor and J_2 next nearest neighbor interactions still occur within the plane while the J_1^* out of plane nearest neighbor interactions occur between thulium atoms of different layers.

Magnetically, the two materials are similar but different. Both show an antiferromagnetic departure from the Curie-Weiss law, a lack of magnetic saturation, and magnetic ordering around 1 Kelvin. However, the difference between the two materials lies in the strength of the magnetic interactions. $TmBr_3$ has much stronger competing interactions that require a stronger applied field to dissipate than TmI_3. This key difference could be the results of crystal field effects. Specifically, inelastic scattering shows only one populated energy mode at low energies for TmI_3 whereas $TmBr_3$ has one and a possible magnetic excitation. Magnetic diffraction also echoes this effect with only one magnetic Bragg peak for TmI_3 but two for $TmBr_3$. The reason behind this behavior could lie in the distances between the magnetic dipole moments. Both structures have similarities, yet differences that arise from increasing the distances between thulium ions. Increasing the interplanar distance can hold the key to tuning and decoupling magnetic interactions for technological applications.

VI. CONCLUSION AND FUTURE WORK

In conclusion, this work fills the gap in literature regarding the structural and magnetic properties of TmX_3 (X=Br, I) and TmOBr. Though comprehensive characterization work has been done on TmX_3 (X=Br, I) and partial characterization on TmOBr —using x-ray diffraction, magnetization measurements, and neutron spectroscopy —, there are still questions as to the exact magnetic structure of the materials presented. Similarly, the characterization of interplanar interactions is limited due to the use of powder samples for all measurements. High quality single crystals can be used to extract interplanar and intraplanar magnetic behavior better than powder averages samples. Therefore, further work needs to be done using single crystals to pinpoint the exact magnetic structure of all materials. In addition, characterization of $TmCl_3$ must be performed in the same manner to fully understand the effects of interplanar and intraplanar magnetic dipole distances on the crystal field and magnetic structures. Future work will be dedicated to completing the characterization of the TmOX (X = Cl, Br, and I) family to truly understand the effects of oxygen ligands and interplanar distances on magnetic behavior in analogy to TmX_3. By completing this work, the magnetism community will expand its materials repertoire, constantly navigating novel phases and materials.

ACKNOWLEDGMENTS

This research was supported by the U.S. Department of Energy, Office of Science, Basic Energy Sciences, Materials Sciences and Engineering Division under award DE-SC-0018660. I'd like to acknowledge my advisor Dr. Martin Mourigal for his advice and support. A special thanks to my graduate mentor Faith Brooks and to graduate student Sathvik Nallapati for their guidance throughout this work.

REFERENCES

[1] J. H. Colwell, B. W. Mangum, and D. B. Utton. Low-Temperature Magnetic Properties of Some Hexagonal Rare-Earth Trihalides. *Physical Review*, 181(2):842–854, May 1969. Publisher: American Physical Society.

[2] S. P Taneja. Magnetic Properties of DyCl3 and HoCl3 Single Crystals. *Journal of the Physical Society of Japan*, 28(5):1167–1170, May 1970. Publisher: The Physical Society of Japan.

[3] K. W. Krämer, H. U. Güdel, B. Roessli, P. Fischer, A. Dönni, N. Wada, F. Fauth, M. T. Fernandez-Diaz, and T. Hauss. Noncollinear two- and three-dimensional magnetic ordering in the honeycomb lattices of Er X 3

(X =Cl,Br,I). *Physical Review B*, 60(6):R3724–R3727, August 1999.

[4] Jie Xing, Erxi Feng, Yaohua Liu, Eve Emmanouilidou, Chaowei Hu, Jinyu Liu, David Graf, Arthur P. Ramirez, Gang Chen, Huibo Cao, and Ni Ni. N\'eel-type antiferromagnetic order and magnetic field–temperature phase diagram in the spin-$\frac{1}{2}$ rare-earth honeycomb compound $\mathrm{YbCl}{}_{3}$. *Physical Review B*, 102(1):014427, July 2020. Publisher: American Physical Society.

[5] D. Hake and W. Urland. Darstellung und Kristallstruktur von LnAl3Cl12 (Ln = Tb, Dy, Ho) und thermischer Abbau zu LnCl3. *Zeitschrift für anorganische und allgemeine Chemie*, 586(1):99–105, 1990. _eprint: https://onlinelibrary.wiley.com/doi/pdf/10.1002/zaac.19905860114.

[6] D. P. Landau, J. C. Doran, and B. E. Keen. Thermal and Magnetic Properties of Ce${\mathrm{Cl}}_{3}$. *Physical Review B*, 7(11):4961–4979, June 1973. Publisher: American Physical Society.

[7] Nashra Pistawala, Suman Karmakar, Rajeev Rawat, and Surjeet Singh. Crystal growth and magnetic behavior of J_eff = 1/2 quantum antiferromagnet CeCl_3, July 2022. arXiv:2207.00629 [cond-mat] version: 1.

[8] J. C. Eisenstein, R. P. Hudson, and B. W. Mangum. Low-Temperature Magnetic Transitions in Some Rare-Earth Trichlorides. *Physical Review*, 137(6A):A1886–A1895, March 1965. Publisher: American Physical Society.

[9] R. B. Clover and R. J. Birgeneau. Magnetic Interactions in CeBr3. *Journal of Applied Physics*, 40(3):1151–1153, March 1969.

[10] W. H. Zachariasen. Crystal chemical studies of the 5f-series of elements. I. New structure types. *Acta Crystallographica*, 1(5):265–268, November 1948.

[11] W P Wolf, M J.M. Leask, B Mangum, and A F.G. Wyatt. Ferromagnetism in gadolinium trichloride. *J. Phys. Soc. Japan*, Vol: 17: Suppl. B-I, 3 1962.

[12] V. Hovi, R. Vuola, and L. Salmenperä. The specific heats of GdCl3, GdBr3, and GdI3 at low temperatures. *Journal of Low Temperature Physics*, 2(3):383–387, May 1970.

[13] F. Varsanyi, K. Andres, and M. Marezio. Canted Antiferromagnetism in Gadolinium Tribromide. *The Journal of Chemical Physics*, 50(11):5027–5030, June 1969.

[14] J. D. Forrester, Allan Zalkin, David H. Templeton, and J. C. Wallmann. Crystal Structure of Terbium Trichloride. *Inorganic Chemistry*, 3(2):185–188, February 1964. Publisher: American Chemical Society.

[15] A. Murasik, P. Fischer, A. Furrer, and W. Szczepaniak. Magnetic properties of TbCl3 determined by neutron scattering. *Journal of the Less Common Metals*, 111(1):177–184, September 1985.

[16] Christian Wessler. *Neutron scattering study of the 2D dipolar magnet ErBr3 and the 2D quantum spin liquid system YbBr3*. Thesis, University_of_Basel, 2022.

[17] H. M. Crosswhite and G. H. Dieke. Spectrum and Magnetic Properties of Hexagonal DyCl3. *The Journal of Chemical Physics*, 35(5):1535–1548, November 1961.

[18] C. P Groen, E. H. P Cordfunke, and M. E Huntelaar. The thermodynamic properties of DyBr3(s) and DyI3(s) from T=5 K to their melting temperatures. *The Journal of Chemical Thermodynamics*, 35(3):475–492, March 2003.

[19] E. H. P. Cordfunke and R. J. H. Blacquière. The system DyBr3 DyI3. *Thermochimica Acta*, 298(1):195–197, September 1997.

[20] Jonathan C. Wasse, Philip S. Salmon, and Robert G. Delaplane. Structure of molten trivalent metal bromides studied by using neutron diffraction: the systems DyBr3, YBr3, HoBr3 and ErBr3. *Journal of Physics: Condensed Matter*, 12(46):9539, November 2000.

[21] Nashra Pistawala, Luminita Harnagea, Sitaram Ramakrishnan, Priyanshi Tiwari, M. P. Saravanan, Rajeev Rawat, and Surjeet Singh. Anisotropic magnetic ground state of single-crystalline quasi-two-dimensional honeycomb antiferromagnet ybi$_3$. *Phys. Rev. B*, 110:104421, Sep 2024.

[22] Jorma Hölsä, Ralf-Johan Lamminmäki, Mika Lastusaari, Pierre Porcher, and Regino Sáez-Puche. Simulation of the paramagnetic susceptibility in rare earth oxychlorides. *Journal of Alloys and Compounds*, 303-304:498–504, May 2000.

[23] S. Mat'aš, M. Mihalik, B. Klemke, and A. Sokolowski. Low Temperature Properties of Selected Kramers Rare Earth Oxychlorides. *EPJ Web of Conferences*, 40:11005, 2013. Publisher: EDP Sciences.

[24] Jorma Hölsä, Manu Lahtinen, Mika Lastusaari, Jussi Valkonen, and Jussi Viljanen. Stability of Rare-Earth Oxychloride Phases: Bond Valence Study. *Journal of Solid State Chemistry*, 165(1):48–55, April 2002.

[25] Jorma Hölsä, Mika Lastusaari, Janne Niittykoski, and Regino Sàez Puche. Interplay between crystal structure and magnetic susceptibility of tetragonal ROBr. *Physical Chemistry Chemical Physics*, 4(13):3091–3097, June 2002. Publisher: The Royal Society of Chemistry.

[26] Jianting Ji, Mengjie Sun, Yanzhen Cai, Yimeng Wang, Yingqi Sun, Wei Ren, Zheng Zhang, Feng Jin, and Qingming Zhang. Rare-Earth Chalcohalides: A Family of van der Waals Layered Kitaev Spin Liquid Candidates. *Chinese Physics Letters*, 38(4):047502, May 2021. Publisher: Chinese Physical Society and IOP Publishing Ltd.

[27] Shuhao Yang, Andrzej Anderko, Richard E. Riman, and Alexandra Navrotsky. Thermochemistry of 3D and 2D Rare Earth Oxychlorides (REOCls). *Inorganic Chemistry*, 61(19):7590–7596, May 2022. Publisher: American Chemical Society.

[28] W. H. Zachariasen. The UCl3 Type of Crystal Structure. *The Journal of Chemical Physics*, 16(3):254, March 1948.

[29] B. Morosin. Crystal Structures of Anhydrous Rare-Earth Chlorides. *The Journal of Chemical Physics*, 49(7):3007–3012, October 1968.

[30] J. H. Colwell and B. W. Mangum. Low-Temperature Heat Capacity of NdCl3 and PrCl3. *Journal of Applied Physics*, 38(3):1468–1469, March 1967.

[31] J. Kotzler, W. Scheithe, K. Knorr, and W. B. Yelon. Neutron diffraction study on magnetic properties of anhydrous gadolinium trichloride. *Journal of Physics C: Solid State Physics*, 9(7):1291, April 1976.

[32] Federico J. Pomiro, Gastón G. Fouga, Juan P. Gaviría, and Ana E. Bohé. Thermogravimetry study of Gd2O3 chlorination. *Journal of Thermal Analysis and Calorimetry*, 122(2):679–687, November 2015.

[33] Xin Wang, Weixiang Hao, Ningzhou He, Xinhua Wang, Yikun Zhang, and Mi Yan. Structural and cryogenic magnetic properties of the REOCl (RE = Ho, Dy, Tb, and Gd) compounds. *Ceramics International*, 50(11, Part B):19838–19844, 2024.

[34] Congkuan Tian, Feihao Pan, Le Wang, Dehua Ye, Jieming Sheng, Jinchen Wang, Juanjuan Liu, Jiale Huang, Hongxia Zhang, Daye Xu, Jianfei Qin, Lijie Hao, Yuan-

hua Xia, Hao Li, Xin Tong, Liusuo Wu, Jian-Hao Chen, Shuang Jia, Peng Cheng, Jianhui Yang, and Youqu Zheng. DyOCl: A rare-earth based two-dimensional van der Waals material with strong magnetic anisotropy. *Physical Review B*, 104(21):214410, December 2021. Publisher: American Physical Society.

[35] Feihao Pan, Jiale Huang, Chenglin Shang, Bingxian Shi, Jianfei Qin, Hongliang Wang, Lijie Hao, Jinchen Wang, Juanjuan Liu, Daye Xu, Hongxia Zhang, and Peng Cheng. Magnetic properties of van der Waals layered single crystals DyOBr and SmOCl, January 2024. arXiv:2401.06741 [cond-mat].

[36] Zheng Zhang, Yanzhen Cai, Jing Kang, Zhongwen Ouyang, Zhitao Zhang, Anmin Zhang, Jianting Ji, Feng Jin, and Qingming Zhang. Anisotropic exchange coupling and ground state phase diagram of Kitaev compound YbOCl. *Physical Review Research*, 4(3):033006, July 2022. Publisher: American Physical Society.

[37] Juan Rodríguez-Carvajal. Recent advances in magnetic structure determination by neutron powder diffraction. *Physica B: Condensed Matter*, 192(1):55–69, 1993.

[38] K. R. Lea, M. J. M. Leask, and W. P. Wolf. The raising of angular momentum degeneracy of f-Electron terms by cubic crystal fields. *Journal of Physics and Chemistry of Solids*, 23(10):1381–1405, 1962.

SUPPLEMENTARY INFORMATION

A. TmOBr Synthesis

Solid state synthesis of TmOBr was conducted using a nitrogen tub furnace and commercially purchased powder reactants Tm_2O_3 (99.99%) and excess NH_4Br (99.9%). The following chemical reaction was conducted to effectively synthesize TmOBr:

$$Tm_2O_3 + 2\,NH_4Br \rightleftharpoons 2\,TmOBr + 2\,H_2O + ...$$

Stoichiometric amounts of each reactant were added to a mortar and ground for approximately 5 minutes or until thoroughly combined. To ensure the reactants reacted completely, 80% excess of NH_4Br was added to the mixture. The resulting mixture was placed in a capped crucible in a nitrogen tube furnace at room temperature and heated to 450 °C for 60 minutes. The temperature was maintained at 450 °C for another 60 minutes before the crucible was heated to 800 °C over 60 minutes. The temperature was maintained at 800 °C for 45 minutes before the furnace was turned off. The system was allowed to cool to room temperature before the crucible was removed and quickly transferred to a glove box. The XRD diffraction profile of the resulting TmOBr compound can be seen in Figure S1.

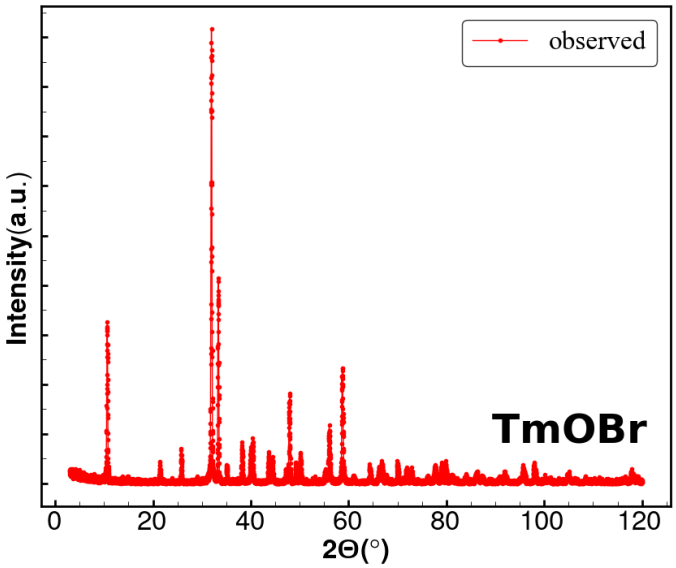

FIG. S1: X-ray diffraction profile of TmOBr (Cu-K_α $\lambda = 1.54$ Å) as synthesized using solid state recipe found in Section A of the Supplementary Information. The material appears to have crystallized into the P4/nmm space group with little impurities from preliminary analysis.

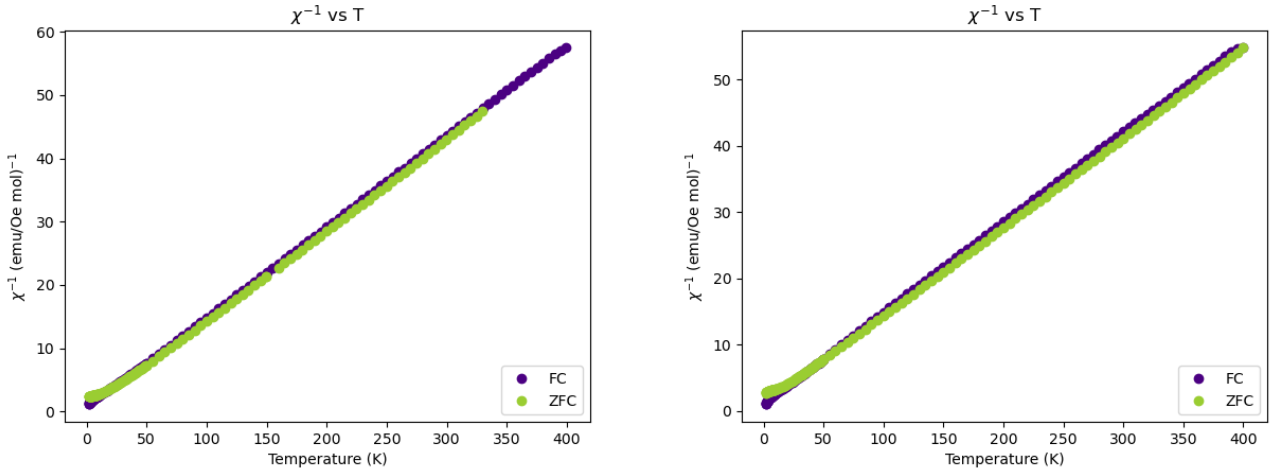

(a) $TmBr_3$ (b) TmI_3

FIG. S2: ZFC and FC magnetization curves as a function of temperature.

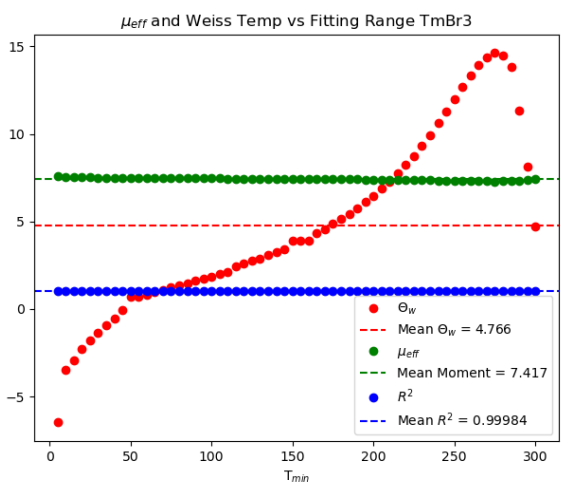

(a) $TmBr_3$

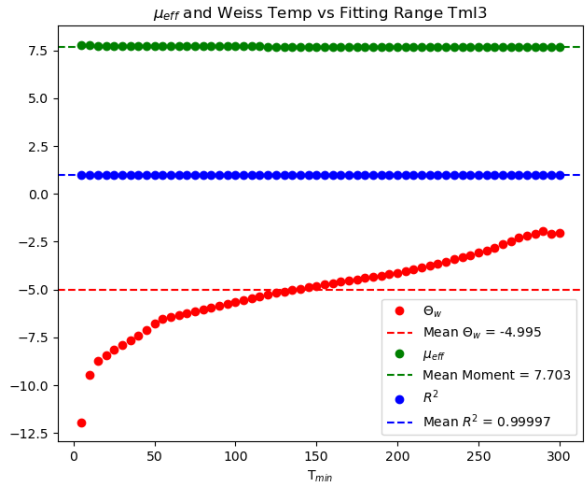

(b) TmI_3

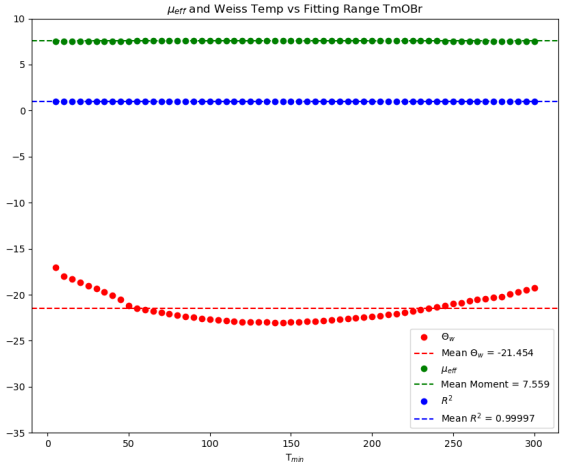

(c) TmOBr

FIG. S3: Fitting parameters as a function of the fitting range. ZFC fata was fit within the [T_{min}, T_{max}] where T_{max} is 350 K for $TmBr_3$ and 400 K for TmI_3